ORIGINAL ARTICLE

Hot embossing of aspherical Fresnel microlenses: design, process, and characterization

João Paulo Colafemina[1] · Marcel Henrique Militão Dib[2] · Renato Goulart Jasinevicius[3]

Abstract

Hot embossing is a technique used to fabricate high-precision and high-quality polymeric components that combines low costs with high aspect ratio fidelity replication. In this study, we manufactured two aspherical Fresnel molds employing the single-point diamond turning process on an electrolytic copper workpiece, one with 10 μm constant height 30 zones and the other with 250 μm constant width 40 zones. The micromachined mold reproduced PMMA convex-plane lens optical quality replicas through the micro hot embossing technique. We used a scanning electron microscope (SEM), spectrophotometry, and non-contact optical profilometer to evaluate the replication fidelity qualitatively: the lens mold and the fine three-dimensional microstructures on the PMMA substrate surfaces. The results of the surface finish of the diamond machined mold sample are in the range of 4.92 nm (areal average surface roughness Sa) and 6.04 nm (areal root-mean-squared roughness Sq), respectively, and the values for the replicas being 4.73 nm and 5.94 nm, respectively. The results demonstrated that the geometry form accuracy obtained of the microfeatures was at the submicron level with little viscoelastic recovery. The surface roughness in the nanometer level got successfully replicated.

Keywords Micro hot embossing · Aspherical Fresnel microlenses · Ultraprecision diamond cutting · PMMA · Viscoelastic recovery · Optical surface finish

1 Introduction and a brief review

Fresnel lenses and diffractive microlens array are typical examples of components that demand absolute control over parameters to get large scale mass production with low manufacturing costs per unit. Fresnel lenses are thinner and lighter than conventional lenses with the same capability. The microfeatures are compacted, formed by an entire concentric ring structure with constant height or constant width. Fresnel lenses have large applications such as concentrated solar power systems, thermal imaging systems, automotive, smartphone flash systems, LEDs, security dispositive, and exceptional cases like X-Ray, satellites, optical instruments, astronomical telescopes, and others [1–4].

Among the replication techniques used to produce micro diffractive optical elements (μDOE) in the polymer, the microinjection molding process is the most suitable and used fabrication process. However, the micro hot embossing technique can offer some competitive advantages such as reduced manufacturing cost, easy operation due to few variable process parameters, and high fidelity for high aspect ratio when small batch production is required. Micro hot embossing of thermoplastic polymers is emerging in the manufacturing areas of optical components and microstructures [5]. In particular cases, such as components with a high aspect ratio, the polymer microinjection process may find difficulties filling microcavities. Consequently, unfilled surfaces show high roughness and wrinkled appearance, generating poor optical response performance of the replicated diffractive optical elements [6].

✉ João Paulo Colafemina
jpcolafemina@ifsp.edu.br

1 Federal Institute of Education, Science and Technology of São Paulo, Sertãozinho, SP, Brazil

2 Federal Institute of Education, Science and Technology of São Paulo, Araraquara, SP, Brazil

3 Precision Engineering Lab, Department of Mechanical Engineering, Engineering School of São Carlos, University of São Paulo, São Carlos, SP, Brazil

2 Aspherical Fresnel microlenses and manufacturing processes

Polymer optics as a working substrate have gained increasing importance in recent years in the fabrication of optical

elements having the price reduced substantially compared to glass-based products and enabling mass production. They compete with traditional glass lenses in various fields of applications. One of the most critical points in the fabrication of polymer optical components is the mold insert required for injection molding or injection compression molding, respectively [7–9].

Spherical lenses generally present longitudinal spherical aberration, which makes light to focus on different positions along the optical axis [10]. Errors of spherical aberrations, such as astigmatism and coma, found in optical lenses made of polymers or glass, are caused by tool manufacturing methods in the production of mold or replicas, generated by tooling errors or plastic behavior like surface stresses during molding, volumetric shrinkage/swelling due to viscoelasticity property of polymers. In polymer lenses, these are considered intrinsic characteristics caused during polymers' replication processing and have currently investigated to reduce or mitigate these phenomena [11–13].

Considering machining the molds, for Fresnel structures with great depth or large diameter, the low rate of material removal becomes a problem in the process's efficiency. Among the several manufacturing cutting processes used to produce optical molds or inserts, photolithography and diamond turning are the two most massive machining methods used to fabricate Fresnel microstructures [14]. Techniques such as polishing do not allow the reproduction of complex geometries, in addition to the high cost of the production chain and the delay in manufacturing time. The LIGA technology or lithography is expensive and time-consuming when the process becomes very complicated and when many hierarchic levels are needed [7].

Diamond turning technology allows fabricating narrow Fresnel zones with spherical or aspherical shape without the need for any conical approach. In this way, single-point diamond turning technology is considered an essential manufacturing technique allowing it to generate surfaces with complex aspherical geometries and, hence, offering convex lenses free from spherical aberration [14].

Ultraprecision machines achieve a positioning accuracy in the nanometer range, which leads to outstanding surface quality and form accuracy. The deterministic nature of single-point diamond turning, handling, and process control is possible due to the development and availability of high-tech machine tools and control technology. These characteristics enable application extensively to complex optics manufacturing, such as reflective elements for guiding laser beams, laser forming systems, aerostatic bearings, or molds for the replication process is just a small extension of parts manufactured with this technology [7].

Moreover, ultraprecision machining with diamond turning creates the possibility of manufacturing lens sizes ranging between size orders of micrometers and millimeters in the same device. Therefore, hierarchical multiscale level-structured surface parts possibly can be produced varying the depth in the micrometer scale of the feature, and otherwise the diameter in the order of millimeters, as the case of both Fresnel microlenses produced in this work [15].

The depth and size of the structure fabricated with diamond turning are limited only due to the diamond geometry size of the tip, typically in a few hundreds of microns to a millimeter [16].

Another essential feature is that single-point diamond turning generates inserts with optical surface roughness, in which roughness (RMS) must be approximately 10 to 20 times less than the wavelength of the light ($\lambda/10$ or $\lambda/20$). Commonly, optical plastic components work close to infrared light, which means that roughness must have to be less than 30 nm RMS [17].

In addition to the quality of the surface's integrity, the roughness also affects the friction factor and, therefore, the flow parameters that favor the filling effect, which is directly proportional to the roughness, which, if higher, requires more significant filling pressure. Few studies investigated micro-scale factors correlating the filling effect to the surface roughness of the mold. Usually, in tiny cavities in the microscale, roughness plays an essential role in the mold's flow behavior commonly neglected when analyzing conventional molding replication. Zhang, Ong, and Lam studied the effects of surface roughness on microinjection molding, and as expected, higher pressure was required to fill the cavity with more elevated surface roughness under the same experimental conditions of thickness and volume [18].

Hot embossing is a cost-effective technique to fabricate high-precision and high-quality plastic microstructures. During thermoforming of polymer, operation parameters such as heating temperature, applied pressure, cycle time, and demolding temperature are easy to control, and uncomplicated optimized process steps to obtain replication with high fidelity [19].

Among the thermoforming process's advantages compared to other manufacturing techniques currently used, two of them were highlighted by Deshmukh and Goswami. First, the residual stresses generated are lower because the polymer's external surface layer in thermoforming is slightly deformed, moving small distances regarding the internal material substrate. Second, the operating temperature range is much lower than other replication processes, which helps decrease plastic shrinkage, and the frictional force resulted from the cooling and demolding process during manufacturing [20].

The principal factors regarding the replication process's production are size, aspect ratio, and surface area. Among these three factors, the most crucial characteristics considered as fabrication process response is the aspect ratios achievable determining the manufacturing constraints for a given process/material [21–24].

Becker and Heim studied the filling of high aspect ratios microstructures using plasticizers and agents. However, release agents allow high aspect ratios, according to the authors, up to 50. These are substances not allowed in the Life Sciences applications due to potential sample contamination. The authors pointed out that the process's main critical parameters are the quality of the mold's surface roughness and the temperature cycle [25].

LIN et al. used a high cycle of 2 h for each run to fully replicate pyramidal patterns having a base width of 30 μm and a height of about 20 μm. Moreover, they found defects, including voids and bumps on a PMMA film due to the demolding process. The authors compare the results with a similar commercial product that uses electroplated nickel as the insert and cycle time of about only 1 min per run. The process fails to produce sharp tips with the micrographs showing rounded edges at the pyramidal pattern peaks, getting an aspect ratio of about only 75% fidelity [26].

Cirino et al. obtained $R_{RMS} \geq 12$ nm roughness by machining with a single-point diamond tool on copper inserts by varying the feed rate from 1 to 20 μm/rev and the depth of cut from 1 up to 20 μm [27]. Observing the images of the top edges of the Fresnel lens of the replicas, they seemed to be flat and rounded, demonstrating that the filling was not entirely successful.

Several authors tried to improve the replication fidelity, increasing the temperature of the trials. However, high temperatures have disadvantages, like difficulty in demolding and significant residual thermal stress due to the different thermal expansion coefficients between the mold and the polymer. The thermal strain warpage suffered by the material of the part due to the residual thermal stress. Hence, it is essential to perform micro embossing at the lowest temperature with acceptable fidelity, especially for large area and high aspect embossing [9, 19].

The behavior of amorphous thermoplastic polymers such as PMMA (polymethyl methacrylate) exhibits significant-high time/temperature-dependent viscoelasticity effect strain response, which is an essential factor and found to be a severe source of replication errors during the hot embossing process [13]. Since polymer behaves like rubber above the T_g, the recovery of its deformation can be exceptionally high, which has significant impacts on the recovery process. The mainly dedicated reported studies of recovery problems to avoid it by optimizing process conditions [8]. Basically, thermoplastic polymers experience two stages of deformation in the whole process: one is a stress concentration and strain hardening stage occurring in heating and embossing steps (creep), and the other, in a similar way, when removing the applied stress, the thermoplastic polymer exhibits a time-dependent recovery of strain back towards its original dimensions, this often is considered as a reversal of creep, that is a time-dependent stress relaxation recovery of strain back towards its actual

dimensions that generate a deformation recovery stage occurring in cooling and demolding steps [5, 28]. This effect would be a manifestation of the shape "memory" of the polymer, and during processing form, it "remembers" its previous shape attempts to return to last geometry [29]. For this work, we will call this phenomenon "viscoelastic recovery."

Experimental results reported by GAO et al. indicate that the embossing temperature has the most significant effect on polymer recovery after demolding under the condition of complete filling. It can cause a relative height error of up to 25% of the designed height. The other variables studied that influence the level of accumulated internal/external stress in the polymer and its corresponding elastic recovery were imprinting time, demolding temperature, imprinting force, and the workpiece's size. The conclusions were that imprinting parameters could be optimized by increasing imprinting temperature, extending the imprinting time, decreasing demolding temperature with the smallest force, and the thinnest thickness of the microstructure selected [13].

Lee, Kang, and Youn reported the influence of viscoelasticity recovery experimentally by measuring the height of a replicated pattern. According to their estimative, the difference in size presented by the replicated reached 100 nm higher than the 10 μm depth of the Ni mold pattern [30].

Liu et al. reported in [12] another exciting result of thermoplastic polymers' viscoelastic recovery behavior. The authors investigated the hyperelastic state properties on PMMA above Tg (T = 120 °C) by comparing experimental and numerical simulation results, and the results pointed out that, by maintaining temperature and pressure for several minutes, the viscoelastic recovery was the reason for polymer continuously filling, which resulted in the elimination of an omnipresent defect during hot embossing called "swallowtails."

Shan, Liu, and Lam studied in [31] the viscoelastic recovery using pyramidal indentations stipulating the maximum depth of 3.0 μm different temperatures. After unloading, the results were 2.34, 2.30, and 2.25 μm, respectively, for indentation at 85, 50, and 25 °C, with the applied force required 113, 132, and 200 MPa, respectively. In these three cases, the instantaneous partial elastic recovery was proportional to its indent depth. They conclude that PMMA substrates that temperature directly affects viscoelastic behavior, playing a critical role in creating permanent cavities with decreased recovery as the temperature increases.

In summary, further investigation is entirely necessary for performing the replication of the 3D Fresnel lens efficiently, analyzing the influence of the viscoelastic recovery effect on the plate-to-plate micro hot embossing process issues. The viscoelastic recovery behavior of thermoplastic polymers in the hot embossing process, hitherto, has not been fully explored yet in microcomponents manufacturing. This phenomenon rarely is reported in the literature of μDOEs manufacturing, and just a few works have related it so far. The

relationship between the hot embossing parameters and its successful performance replicating micro and nanofeatures is still open to contribution.

This study contributes to understanding the engraving characteristics in micro and nano-level manufacturing of micro diffractive optical elements (μDOE) using a series of hot embossing experiments. This work will demonstrate the development of a diamond turning technique used to obtain optical mirrored surface finishes (extremely low roughness) on the manufacturing of electrolytic copper inserts of two fine microstructures of Fresnel lenses, one with constant height and another constant width. The performance of the mold surface and the PMMA thermoformed replica was analyzed qualitatively and quantitatively comparing dimensional measurements between both, evaluating the surface finish and the filling effect of the material inside the narrow zones of Fresnel, finding out the side effects of the viscoelastic recovery, revealing the impacts of the fidelity on it.

3 Experimental details

3.1 Design of aspheric Fresnel microlenses

We developed the computational code in Visual Basic language, called LF2020 [32], to construct the two different types of diffractive lenses used in this work. The first microlens is in Fig. 1a. It is a convergent convex aspherical Fresnel lens designed to have a constant height of 10 μm (denoted as FrCH10), with a diameter aperture D = 24 mm, 30 zones, the focal distance of 480 mm, and f/# = 20. The second microlens, demonstrated in Fig. 1b, is a convergent convex aspherical Fresnel lens designed to have constant width of 250 μm (denoted as FrCW250), with a diameter aperture D = 20 mm, 40 zones, have a focal distance of 70 mm, and f/# = 3.5. The LF2020 software resolves the coordinate points (X, Z) to generate the profile mold reliefs to be transcribed for the ASG -2500 ultra-precision CNC lathe. The program provides the surface area and lens volume to calculate the surface area/ volume ratio, as shown in Fig. 1. All these paraxial parameters are described in Table 1 and were determinant for the construction of the microlenses. Both lenses operate in paraxial domains having an aspherical normalized phase profile, and the refractive index is 1.49, calculated for a determined shift phase module.

3.2 Inserts manufacturing

The ultraprecision machine tool used for the cutting tests was the Aspheric Surface Generator 2500 (Aspheric Surface Generator 2500), from RANK PNEUMO (Precitech Components). It is a machine tool specially designed for both turning and ultraprecision grinding. This machine has some

basic requirements like ultra-precise positioning control with 10 nm positioning accuracy calibrated and certified by the manufacturer, a cast iron base, thermally free of tension isolated from external vibrations through passive pneumatic insulators mounted cinematically on a welded steel structure to provide high stiffness. The spindle bearings are aerostatic to provide turning accuracy, axial and radial rigidity compatible with the precision the equipment proposes.

The sharpness gave by the natural monocrystalline diamond cutting tools used in this work allowed to remove material in submicrometric cuts thicknesses, as shown in Fig. 2. This tool type is half radius tool - left hand radius with a 100-μm nose radius. Figure 2a shows the SEM images of the diamond tool tip detailing the cutting edge of the cutting tool, which has unique geometry to allow Fresnel lenses' construction. Figure 2b, obtained from SEM with × 4000 magnification, is the possible note that the cutting edge has perfectly defined geometry, very sharp without any defects.

Table 2 listed the experimental conditions, tool geometry, and optical element mold insert fabrication used at the tests. The material used for the insert samples was the commercially available nonferrous substrate of 99.99% of purity electrolytic copper, with a 1″ diameter mold.

In this way, the machining strategy employed to generate the Fresnel zones mold cavity was a sequence of ten passes for FrCH10 and FrCW250, keeping dc = 1 μm and f = 2,5 μm/rev, as schematically shown in Fig. 3. This diamond tool tip geometry allowed cutting very sharp vertical sidewalls to generate the smooth mirrored surface required. The machining operation for a Fresnel zone consists of two steps. First, the tool starts fed the path from the center of the mold (Z-axis), and then the device moves simultaneously (XZ-axis) following the micro-Fresnel profile feeding to the outer region of the workpiece, whereby an aerostatic spindle rotates at 1000 RPM. During all the machining tests, the cutting fluid we used the synthetic oil Alkalisol 900, pulverized in the form of mist on the interface tool/workpiece, used to lubricate, cool, and throw away the chips to do not damage the surface.

3.3 Hot embossing

Figure 4 shows the closed-die thermoforming apparatus scheme. Closed-die forming has better properties concerning open die forming like dimension accuracy, high production rate, good reproducibility, prevent the bulging of the samples, and improves the filling effect of the PMMA. The device consisted of placing the master mold (with the microstructures) attached to the upper plate and a polished insert at the lower plate. The experiment sequence involves four steps: preheating/preloading, holding embossing pressure, cooling, and demolding. It was unnecessary to preheat the polymer because the experiment's method applied is the non-
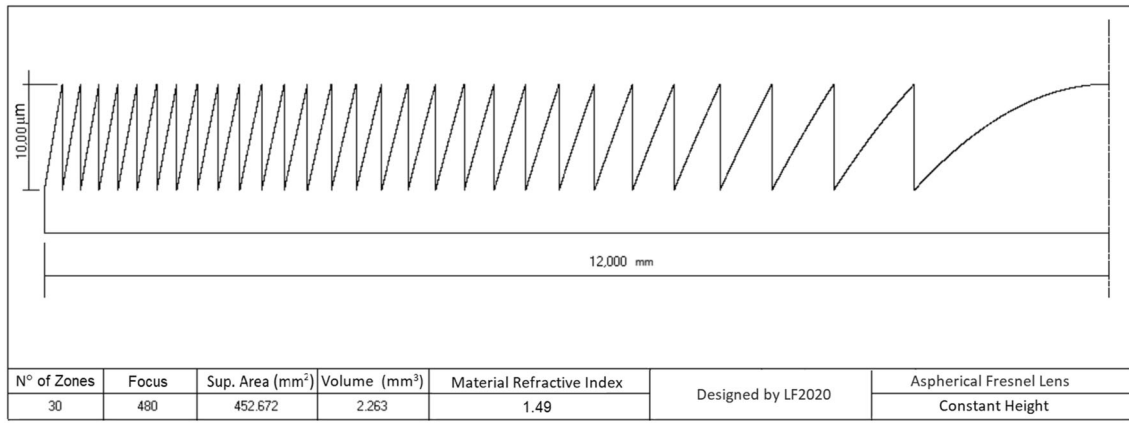
(a)
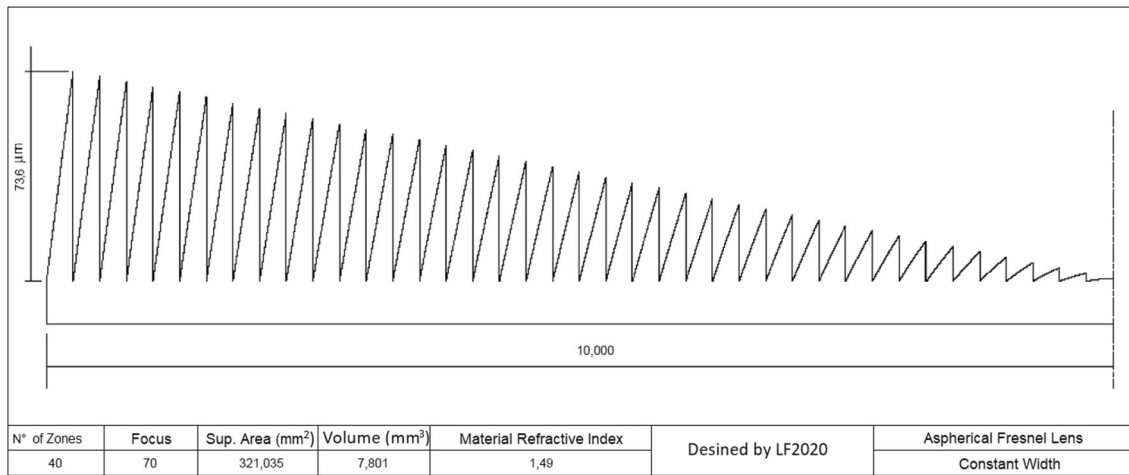
(b)

Fig. 1 Design in LF2020 of Fresnel microlenses with aspheric normalized phase half profile (**a**) Fresnel constant height 10 μm named FrCH10 (**b**) Fresnel constant width 250 μm named FrCW250

isothermal hot embossing, which means the mold heating at different substrate temperatures.

At the initial level, the polymer is at room temperature. In this way, we put the working material in the form of PMMA pellets placing it in the lower mold. Figure 4a shows the hot embossing sketch and the device in Fig. 4b.

The polymer was soon heated from room temperature above its glass transition temperature (Tg PMMA = 106 °C) using a resistance until it reached 120 °C, as shown in Fig. 4c.

A 100 BAR preload applied to the polymer, displacing the upper mold during the heating phase. The load stabilized at the determined time of approximately 5 min and reaching the hot embossing temperature. The loading increase to 150 BAR, the remaining 15 min established known as hot embossing time or holding pressure.

The cooling started to get the temperature below Tg (approximately 5 min) of the polymer. Then, we decrease the loading applied and finally carried out to demolding, obtaining the profile transferred from the reverse microstructures of the mold printed on the substrate of the part Fig. 4d.

Table 1 Paraxial parameters of aspheric Fresnel microlens

Geometry	Aspheric surface radius (mm)	Concavity	Depth of zone z (μm)	φ (mm)	Focus (mm)	f/#	Diopter
Constant height	235	Convex	10	24	480	20	2
Constant width	34.3	Convex	Small=0.93 Big=73.6	20	70	3,5	15

Fig. 2 SEM micrograph of monocrystalline single-point diamond tool half radius tool - left hand radius. **a** General view of the half radius diamond tool tip; **b** Extremely sharpened cutting-edge geometry higher magnification
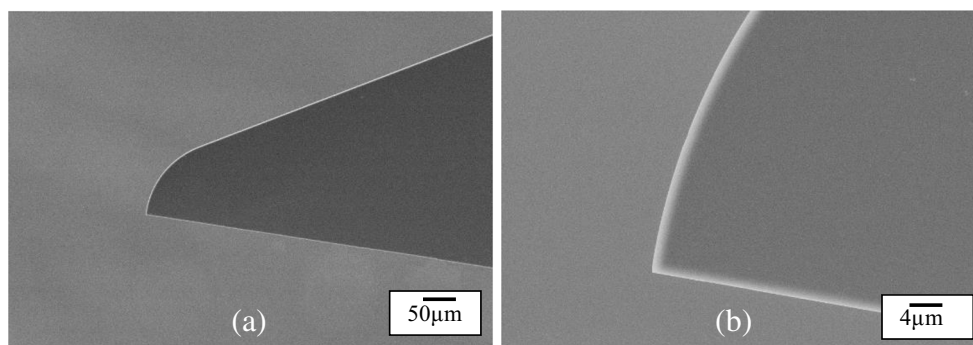
The embossing pressure applied was continuously checked to keep constant during embossing pressure until cooling to avoid shrinkage and warpage caused by the copper mold's mismatch thermal expansion coefficients and the polymer's.

3.4 Metrology

This work used a spectrophotometer, 3D no contact optical profilometer, and scanning electron microscope (SEM). Only SEM does not adequately characterize the surface. The non-contact optical instruments were selected to examine a workpiece's surface for acquiring a cross-sectional profile or areal topography data of the surface [33]. We use the non-contact optical profilometer to determine the lens's aperture diameter and its sagittal height accurately, preventing damage to the part, which is why its use was intensive in this work.

For this reason, the Veeco® Wyco NT1100 non-contact optical instrument aids us in the measurements of the fidelity replication of the copper inserts and lenses produced. This equipment has a subnanometric vertical resolution (Angstrom 0.1 nm) in all magnifications. It uses white light interferometry for high resolution of 3D surface measurements, from subnanometric roughness to millimeter steps. The instrument makes measurements through Vertical scanning-interferometry (VSI) or phase-shifting interferometry (PSI). For mirrored surfaces, phase-shifting interferometry (PSI) is the best option. That is the reason chosen to measure roughness in the experiments. Unlike this, to measure the height and width of the microstructure manufactured on insert and replica, the vertical scanning-interferometry (VSI) technique was employed because it gets a broader range of measures to make it feasible the surface profile and then plotted and analyzed by Vision® software. All data obtained by scanning electron microscope (SEM), spectrophotometry, and non-contact optical profile were determined quantitatively and qualitatively to compare the parameters: filling ratio values, surface roughness, and transmittance.

Table 2 Diamond turning conditions of the copper insert

Workpiece	Cu electrolytic
Lens diameter	24 mm FrCH10 / 20 mm FrCW250
Zone depth/width	10 μm constant height-width variable
	250 μm constant width-height variable
Cutting tool	Waviness < 0.25 μm over 55° excluding elliptical form
Material (Contour Fine Tooling®)	Natural monocrystalline diamond
Nose radius (μm)	100
Tool included angle	30°
Tool rake angle	0°
Tool front clearance angle	10°
Shank	6.35×6.35×51 mm
Cutting conditions	
Depth of cut	1 μm
Feed rate	2,5 μm/rev
Spindle rotation	1000 RPM
Cutting fluid	ALKALISOL 900 mist ±100 ml/h

Fig. 3 Machining strategy applied to the fabrication concave Fresnel lenses mold cavity: a schematic model for Fresnel microlenses structure cutting
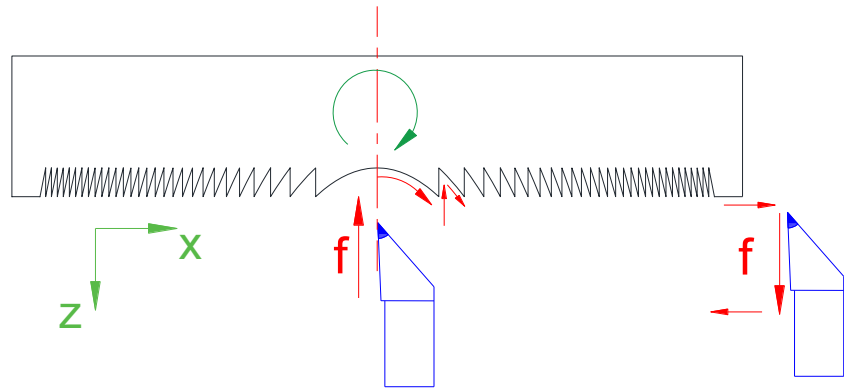
4 Results

4.1 Hot embossing trials

The parameters chosen to execute the trials of the thermoforming technique for the complete filling of the microstructure were a temperature above the glass transition of PMMA of T = 120 °C and hot-embossing pressure of 150 BAR accomplished in a total cycle time of about 25 min. This combination resulted in a fully coalesced lens replica in the hot embossing process, as shown in Fig. 5a. Attempts to decrease the cycle time have not been successful. Figure 5b shows that the

PMMA pellets' coalescence did not occur, with microcracks remaining throughout the lens. Figure 5c shows the detail of a microcrack in the middle of the Fresnel zones, caused by the material's lack of coalescence.

4.2 Aspherical Fresnel lenses: morphology, roughness, and fidelity

Figure 6 shows SEM micrographs of the concave machined electrolytic copper mold surface of the aspheric FrCH10 (Fig. 6a, b) and its respective convex PMMA replica profile (Fig. 6c, d). Figure 6a shows the regularly concentric zones

Fig. 4 Schematic diagram of hot embossing closed-die forming stages used to replicate PMMA Fresnel samples. **a** Preheating and preloading sketch, **b** hot embossing device, **c** embossing holding pressure, and **d** sample demolding
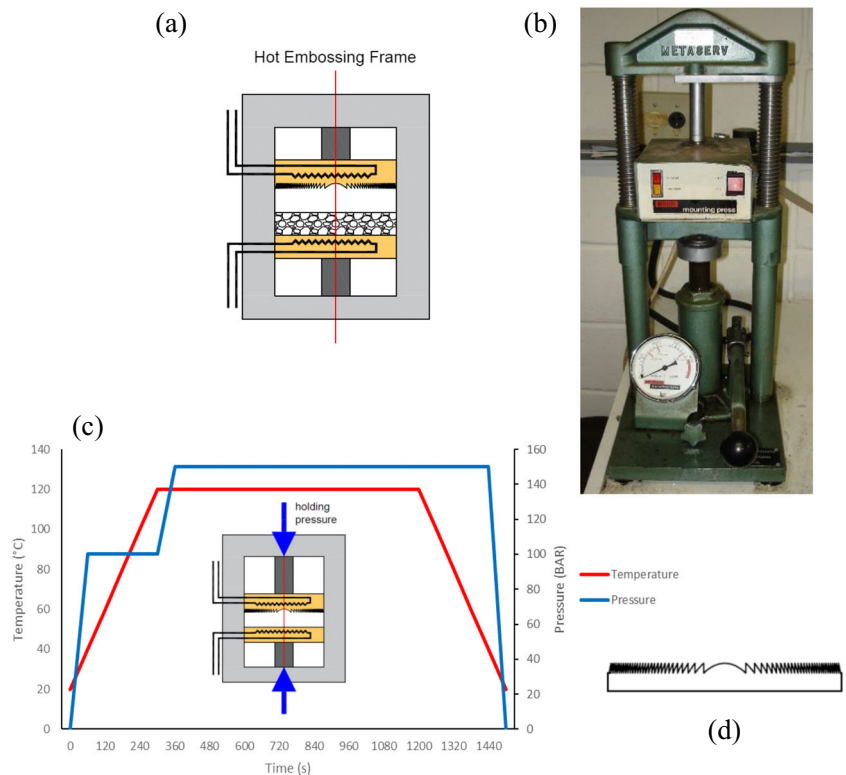
Fig. 5 Hot-embossed Fresnel lens. **a** Lens fully coalesced. **b** Lens incomplete coalesced. **c** SEM detailing a crack between the Fresnel zones formed due to the lack of coalescence of the material

(a)   (b)   (c)
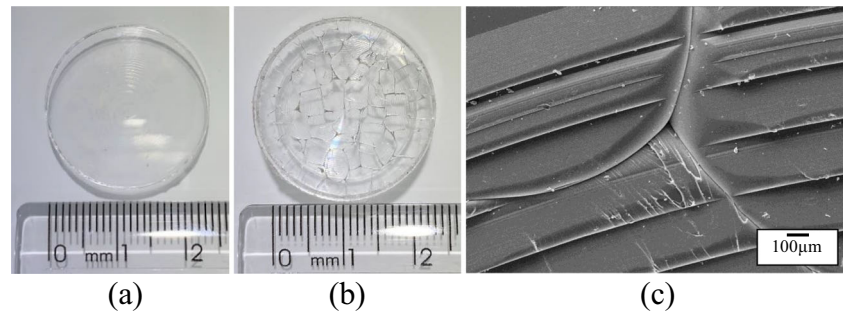
very well performed. Figure 6b shows one zone step (10 μm) that is very straight with a sharp vertical edge, burr formation free, and an exceptionally smooth mold surface. The investigation shows that burrs can be minimized by optimizing the cutting parameters where cutting speed only has a minor effect, while undeformed chip thickness affects the height of the burrs significantly [15]. Our result indicates that the diamond turning conditions strategy used in the experiments was suitable, reflecting directly in the chip formation resulting in uniform width and thickness of the ribbons, as shown in Fig. 7.

Similarly, Fig. 6c depicts SEM micrographs of the PMMA sample surface of convex aspheric FrCH10 replicated by hot embossing technique showing like the mold that the replicated concentric zones on PMMA was well done. Figure 6d is an SEM detailed view of a zone step (10 μm height) showing a straight and vertical step sharp edge, indicating that hot embossing process parameters used in the experiments were suitable. Hence, the replication fidelity transfer ratio was

outstandingly determined since the zones in the picture look wholly fulfilled.

Figure 7 shows SEM micrographs of the electrolytic copper chips removed during diamond turning of the aspheric Fresnel structure. Figure 7a shows a continuous ribbon-like chip. The width and thickness of the ribbons are very uniform, indicating that the cutting process was stable. Figure 7b shows the lamellar structure on the free surface of the chip. This lamellar structure is typical of ductile metals response to cutting and occurs due to shear plane deformation approximated by a series of parallel plates sliding against one another to form the chip. Another essential factor observed in Fig. 7c is the continuity of chip deformation in its posterior part in the function of the tool's intense shear stress introduced. The plastic deformation was continuous since the material is pure, reflecting an excellent surface finish on the mold sample.

The roughness measurements were evaluated using a non-contact optical instrument three-dimensional profilometer and

Fig. 6 SEM micrographs characterization of the aspheric FrCH10 profile. **a** General view of concentric Fresnel zones machined on electrolytic copper mold; **b** Sharp zone step mold; **c** General top view of concentric Fresnel zones PMMA hot-embossed replica; **d** Sharp zone step PMMA replica

(a)   600μm   (b)   10μm
(c)   600μm   (d)   10μm
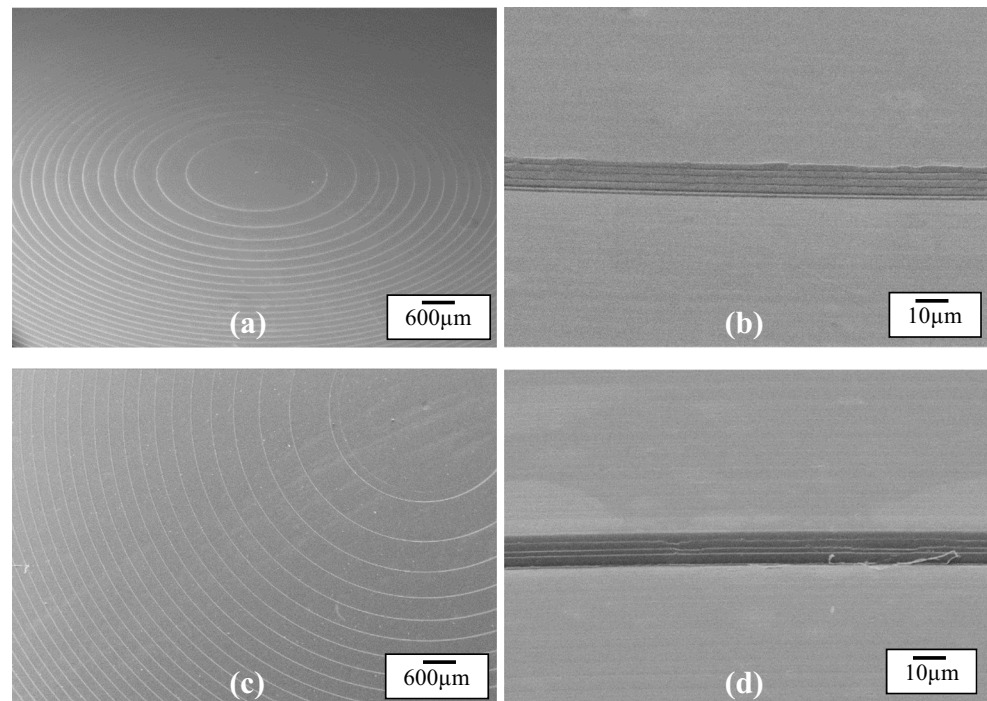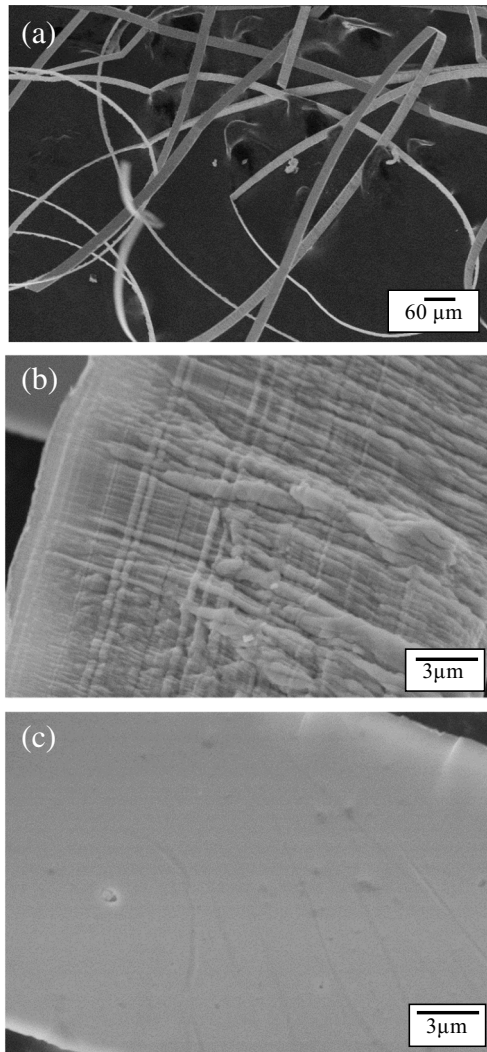
Fig. 7 **a** Electrolytic copper slightly curled ribbons chip machined with diamond tool. **b** Top of the chip showing the lamellar structure. **c** Bottom of the chip showing the plastic deformation imposed by the single-point diamond cutting tool

taken by using the phase-shifting interferometry (PSI) technique. This method accurately measures a smooth surface using a piezoelectric transducer system (PZT), which linearly moves the objective, a small known amount to cause a phase shift between the objective and sample surface. Albeit this technique limitation, it was possible to measure the mold and PMMA replica at the flat plane and the aspheric center of the lenses to compare both results as depicted in Fig. 8.

Figure 8a depicts a mirror-like finish with the roughness measured on a flat part of the upper plate electrolytic copper surface diamond-turned showing a low areal surface average roughness of Sa = 4.92 nm. The respective values of areal root-mean-square roughness (Sq) and maximum areal roughness (St) measured were 6.04 nm and 40.91 nm, respectively. Similarly, the roughness measured on a flat part of the PMMA replicas shown in Fig. 8b depicts the 3D image. Little smaller values were obtained compared to the mold results, replicating

extremely low surface roughness. Therefore, the average roughness (Sa), root-mean-square roughness (Sq), and maximum roughness (St) were 4.73 nm, 5.94 nm, and 39.33 nm, respectively. As seen in the literature previously [17], a device working in wavelength of 632.8 nm, this surface finish corresponds to a ratio of approximately λ/106. This level in practical use is acceptable in most fine optical components applications.

The roughness results of the aspherical center of the copper mold are in Fig. 8c. The roughness average (Sa), root-mean-square roughness (Sq), and maximum roughness (St) was 8.34 nm, 10.61 nm, and 91.30 nm, respectively. Similarly, the aspherical center of the PMMA hot-embossed lens depicted in Fig. 8d shows a little smaller roughness than the mold. The values were 6.97 nm, 8.86 nm, and 71.84 nm for average roughness (Sa), root-mean-square roughness (Sq), and maximum roughness (St), respectively.

Although the same machine conditions on the flat part and an aspheric center part, including the use of sphere and tilt filters on Vision software.

The curvature's effect influenced producing higher values at the lenses aspheric center than the flat part results. Nevertheless, the roughness results are in good agreement as required for optical applications, proving that diamond turning conditions and the micro hot embossing parameters used were suitable for aspherical geometry lenses.

Figure 9 shows the evaluation of the 3D image surface finish of the polished insert used as the lower plate in the trials. The mirror-like finish obtained for average roughness (Sa), root-mean-square roughness (Sq), and maximum roughness (St) was 2.74 nm, 3.54 nm, and 32.18 nm, respectively. For PMMA replica, the outcomes were even better with 2.43 nm, 3.03 nm, and 27.11 nm, respectively. The results were exceptionally low roughness, getting the bests surface results of this work.

According to the values shown in Figs. 8 and 9, all measurements realized at 3D non-contact profilometer indicated that the roughness average (Sa), root-mean-square roughness (Sq), and maximum roughness (St) value of hot-embossed Fresnel microlens replica was a little smaller than that of the electrolytic copper mold insert. This trend follows the literature [34], and these decreases in the roughness values of the replicas occur after the molding process because some micro and nano features lose fidelity during the replication process.

This low surface roughness enables the high performance of transmittance light in an extensive range of spectrum wavelengths. Low roughness generates a mirrored surface, which improves the transmittance of light because it avoids its scattering of light. In this way, because of these excellent surface finish obtained in the Fresnel lens replicas, a high transmittance was found, ensuring around 90% along all visible spectrum, as shown in Fig. 10, got measured by a spectrophotometer.

Fig. 8 Areal surface roughness measured by non-contact optical profilometer; **a** 3D image from the flat portion of the mold; **b** PMMA roughness flat part; **c** 3D image of the aspheric center part of the mold; **d** Roughness of the aspheric center part of the PMMA hot-embossed
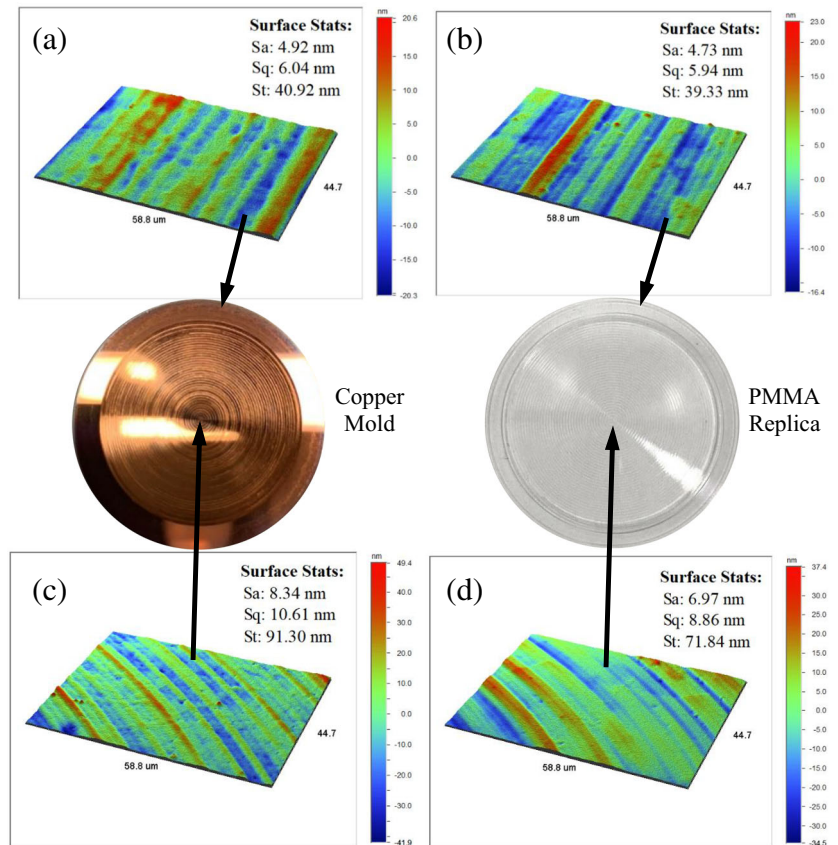

The non-contact optical three-dimensional profilometer instrument aided in investigating the replication fidelity. We set up the vertical scanning-interferometry (VSI) technique to get a broader range of profound measures.

The surface topography of the aspheric Fresnel lens mold depicted in Fig. 11a shows the concave 3D topography general view of the diamond-turned surface half profile of the electrolytic copper mold. Figure 11b presents the respective two-dimensional cross-section of the Fresnel zones profiles displaying the average height accuracy is in the submicron level; it can observe that all vertical zones profile shows the steeps and sharp vertical edges are around 10 μm height.

Similarly, Fig. 11c shows the convex 3D topography general view of the thermoformed PMMA replica showing the

mold's 30 zones reverse profile. Figure 11d exhibits the two-dimensional cross-section of the Fresnel zones profiles; in this image, all vertical zones profile shows a steep and highly sharp edges zones around 10 μm height average. Hence, the complete filling occurs without damage at the peaks' demold stage, and the average height accuracy was at the submicron level. The height and width designed for the first zone were 2.188 mm in width and 10 μm high. The measured values of the electrolytic copper mold on the 3D profilometer obtained were 2.1885 mm and 9.9232 μm, respectively, showing a difference of 0.0768 μm height within the range of the machine tool positioning error. The last zone's designed size was 0.2 mm width and 10 μm high, and the measurements obtained for width and height were 0.2024 mm and 10.009 μm,

Fig. 9 3D image surface finish. **a** Electrolytic copper polished lower plate mold, and **b** PMMA replica
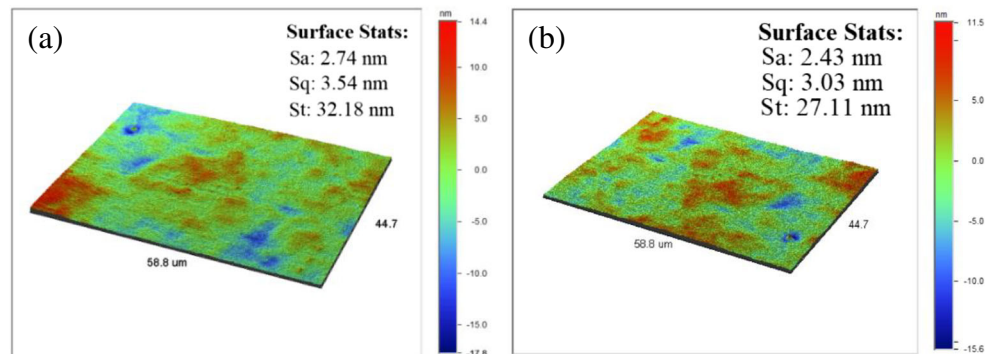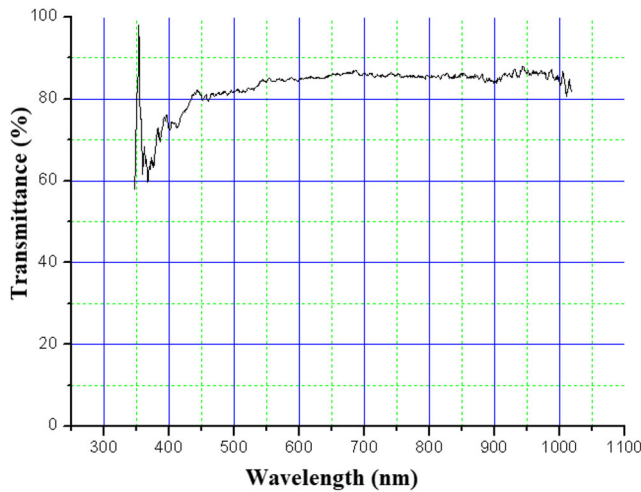
Fig. 10 Transmittance of PMMA hot-embossed Fresnel microlens

respectively. These results show the deterministic nature of the single-point diamond turning process.

The same measurement was carried out for the Fresnel zones PMMA replica's height and width compared to the diamond-turned copper mold to respond in terms of replication fidelity accuracy. The width and height of the first zone of the lens measured was 2.1883 mm and 10.0042 μm, respectively; the height value corresponds to a difference from the mold values in the order of 0.081 μm higher. For the last zone

in both, the replication experiment results obtained were 0.2024 mm width and 9.9345 μm height. The height value corresponds to a difference from the mold values in the order of 0.074 μm lower. This high-fidelity ratio obtained is attributed to the outcome of extremely low surface roughness of the inserts, as shown in the literature. This good roughness ensures that the filling effect is more accessible, combined with adequate hot embossing technique parameters, also known as high-quality plastic microstructures replication.

Thoroughly analyzing each zone, higher values were founded in some replicated samples concerning the mold peak measurements related to a viscoelastic recovery behavior. Since the loaded material for an extended period and viscoelasticity is a molecular rearrangement phenomenon, portions of the polymeric chains change positions when stress is applied. When removed the applied stress, the accumulated back stresses will cause the polymer to return to its original form [35]. According to this, the recovery behavior observed occurs due to the stress relaxation around the sharp peaks. Figure 12 shows the schematic temperature and pressure cycle profiles during the replication process and the PMMA recovery after the cooling and demolding stage. As a result, a polymer's total deformation of an under applied mechanical stress will contain permanent deformations and recoverable elastic deformation on removing the stress. Thus, during the demolding stage, stress relaxation occurs. Hence, viscoelastic recovery happens

(a)

(c)

(b)

(d)
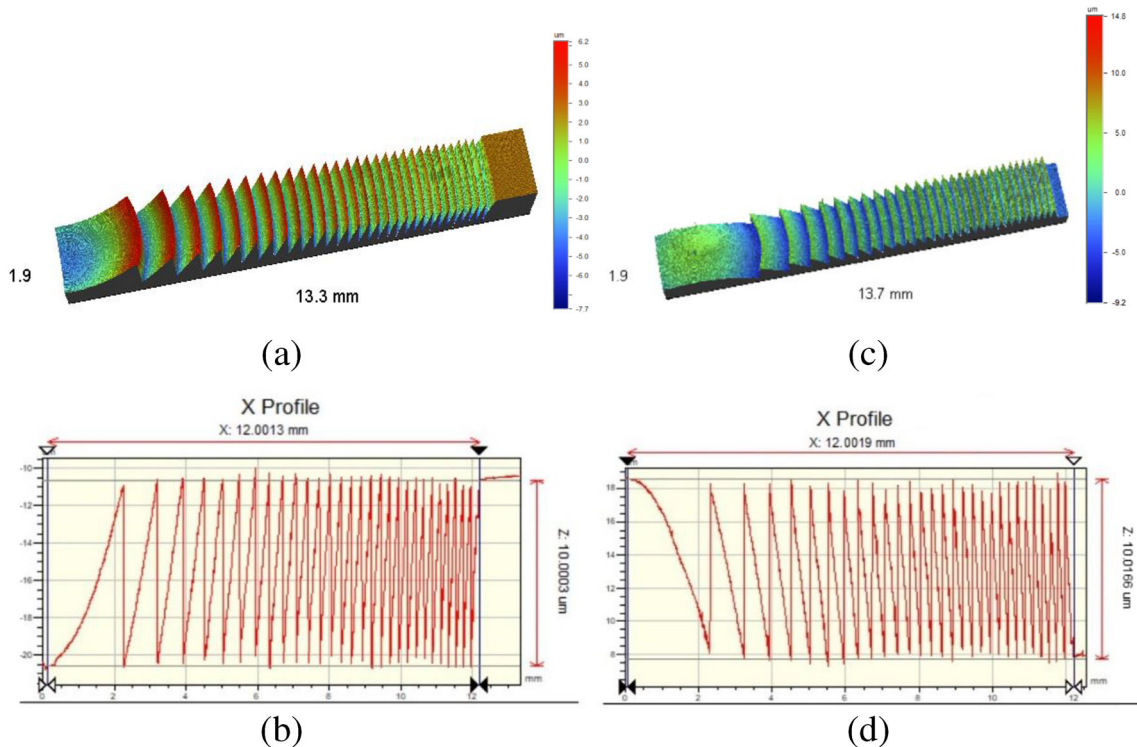
Fig. 11 Characterization of the aspheric FrCH10 lens profile of mold and replica with non-contact optical instrument three-dimensional profilometer. **a** 3D general view of 30 Fresnel zones half profile electrolytic copper mold. **b** Respective profile showing 10 μm constant height of the mold. **c** 3D general view of 30 Fresnel zones half profile of PMMA replica. **d** Replica's profile shows 10 μm constant height of FrCH10 PMMA

Fig. 12 Temperature and pressure cycle profiles during the replication process and the PMMA viscoelastic recovery after cooling and demolding
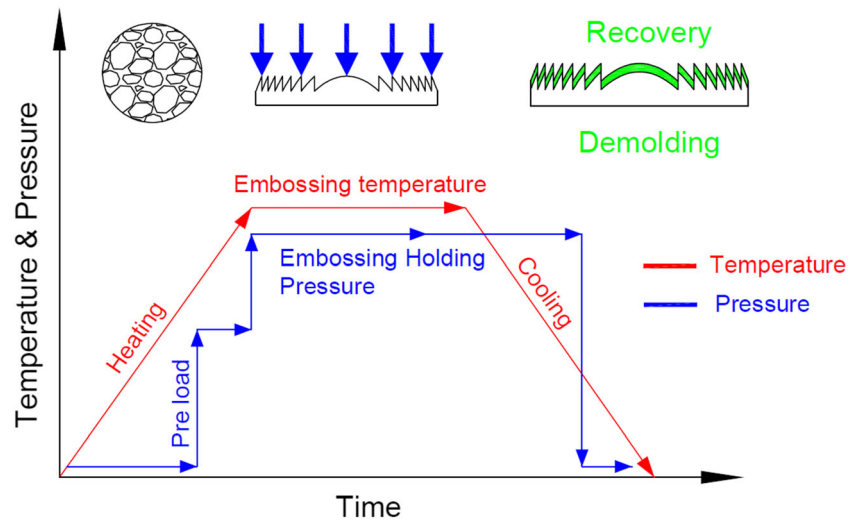
significantly, and relaxing the stresses increases the cross-section, causing variation in the height of some crest's zones in a size range of few nanometers higher sometimes.

The viscoelastic recovery in the replication process was evaluated quantitatively regarding the replica's dimensional variations concerning the mold. To this end, two equations for the measurements, fidelity height ratio, represented by Eq. (1), and fidelity width ratio, defined by Eq. (2). Equations (1) and (2) give Fresnel microstructure fidelity ratio, calculating the relative dimensions difference between the replica and the mold, basing on the mold sizes.

$$F_{\text{HEIGHT}} = \left[1 - \frac{\left(H_Z^{\text{MOLD}} - H_Z^{\text{Replica}} \right)}{H_Z^{MOLD}} \right] \times 100 \qquad (1)$$

$$F_{\text{WIDTH}} = \left[1 - \frac{\left(W_Z^{\text{MOLD}} - W_Z^{\text{Replica}} \right)}{W_Z^{\text{MOLD}}} \right] \times 100 \qquad (2)$$

Where H_z^{mold} is the height measurement of Zth Fresnel zone of the mold insert, H_z^{Replica} is the height gauged of Zth Fresnel zone of the PMMA replica, and W_z^{mold} is the width measurement of Zth Fresnel zone of the mold insert, W_z^{replica} is the width measurement of Zth Fresnel zone of the PMMA replica. Therefore, it was possible to plot Fig. 13, which depicts the results of height and the width fidelity ratio, for each one of the thirty Fresnel zone of FrCH10. The width fidelity ratio of the zones was close to 100% along all zones. On the other hand, the height fidelity ratio presents a more up-and-down variation along the 30 Fresnel zones, sometimes showing values higher than 100% for most zones. This behavior is inherent to the viscoelastic property where polymer recovery takes place after stress release. However, it is worth noticing

that this discrepancy was at the nanometer level. It ranges from a few dozens to hundreds of nanometers. For example, when the ratio reaches 106%, it corresponds to 600 nm in the fifteenth lens zone. A linear trend was traced along the plotted values to show the decreasing trend of height fidelity and realized that the polymer chains have more challenge to fill these narrow zones for higher aspect ratio (external zones of the lens). The outmost zones have a higher aspect ratio, consequently, results in the lowest fidelity value of the plotted graphic hence found for these conditions, the lower fidelity value achieved about 98%, which corresponds to a peak of 200 nm shorter than the nominal value.

Replication errors are mainly incomplete filling during imprinting, polymer recovery after demolding, and transfer error by manufacturing inserts. Besides tooling errors, surface tension causes recovery and volumetric shrinkage, and they are the most significant error sources. According to previous studies [17], the accuracy with which an optical surface molded is mainly influenced by the surface stresses, in the corners and edges, where the ratio of surface area/volume is locally high, and due to this fact, the generated surface tension in micro components it will cause non-uniform retraction or warpage of the microstructures. Surface tension and volumetric shrinkage may, however, actually aid in the production of an accurate surface. Based on the preceding phenomena highlighted, the LF2020 program provides lens surface area $S = 452.672$ mm^2 for FrCH10 and the respective volume $V = 2.263$ mm^3, making it possible to calculate the surface/volume ratio, that was found for this case 195.967 mm^{-1}. This ratio is a critical factor because the superficial skin layer defines the surface area/volume behavior of the lens material's mechanical and optical properties.

In contrast, in the lens with a lower ratio surface area/volume, the action is majority defined by the substrate. Therefore, it will directly influence the mold filling behavior, directly influencing parts produced in the micro-molding. It

Fig. 13 Graphic of width and height fidelity ratio of the 30 zones FrCH10
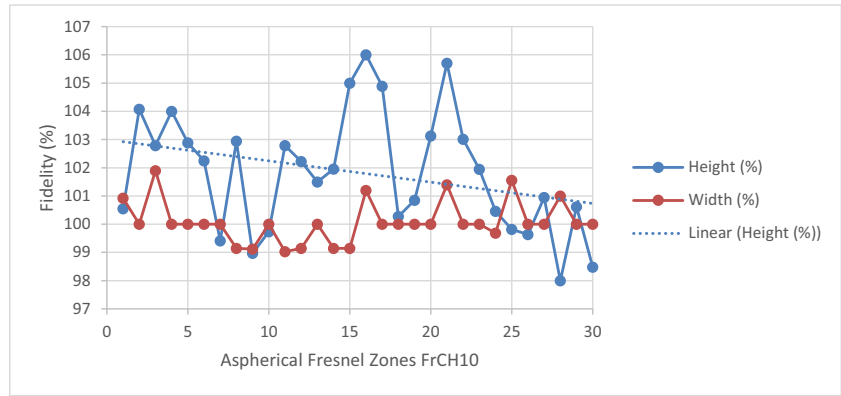

solidifies faster than in conventional molding due to the small polymer volume and the high surface/volume ratio typical of molding micro parts.

The graphic plotted in Fig. 14a determines the microlens geometric influence by overlapping both reliefs (mold and replica) of the first three zones obtained got by the exported points of the 3D non-contact profilometer. The PMMA profile is always above of mold profile as viscoelastic previously exposed reasons. Each zone profile of the mold and replica was strictly analyzed, and particularly, at the profile number

one zone, it was noticed inside the black circle highlighted that the warpage occurred. Warpage occurred due to the differences in shrinkage over the whole thin residual layer. This contraction occurs by the difference of the melt state's polymers density and then cooled rigid form, and depending on part stiffness, causes the part to deform or change shape.

Two factors caused the warpage in the larger protrusion at the center of the μDOE pattern. First, is that in the first zone, the superficial layer requires a lengthly displacement of polymer flow, causing much larger internal stress accumulated at

Fig. 14 Profile of FrCH10 mold and replica. **a** First zones, and **b** one zone magnified showing the polymer viscoelastic recovery phenomena of PMMA
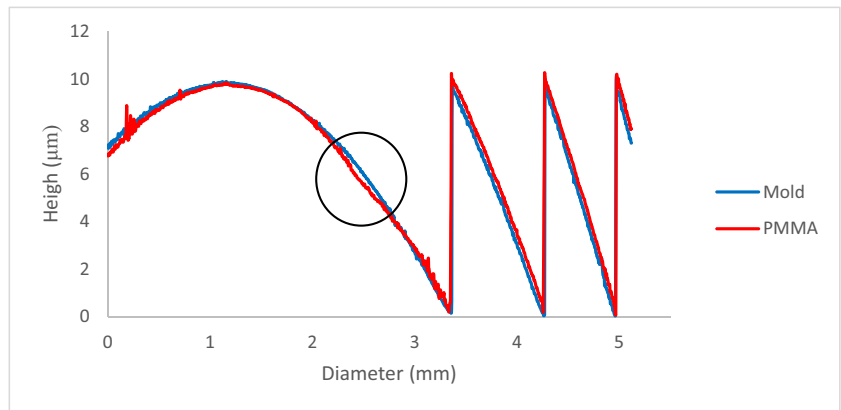
(a)
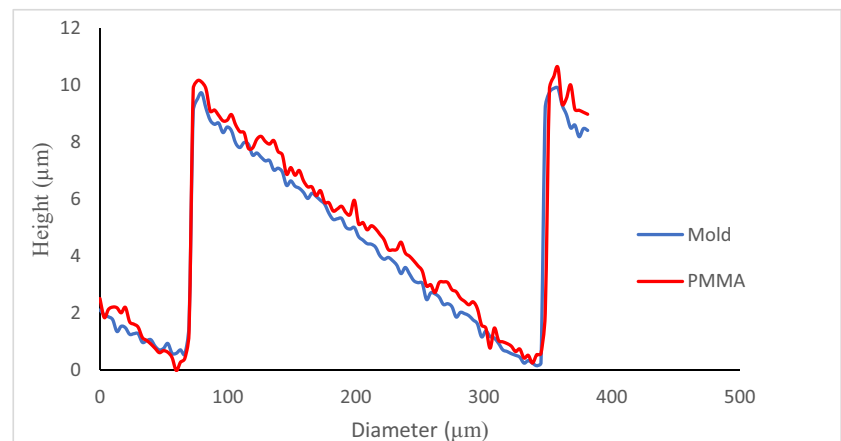
(b)

the center, combining with the highest ratio of the surface area/volume that is 195.967 mm^{-1} for this case, more surface tension will happen whereby will affect the dimension accuracy. Second, due to a more significant amount of substrate material, a highly gradient temperature during the process cooling step is formed, causing unequal residual stresses at the superficial layer. The rapid cooling in the outer region causes the retraction of the polymeric material, making it even more difficult to add material into the microcavities, worsening the distortion of the lens profile by shrinkage effect because of a difference in the temperature coefficients of tool and substrate material, affecting the optical performance due to the appearance of the optical aberration (Fig. 15).

The graphic of Fig. 14b shows one zone magnified, showing the polymer viscoelastic recovery phenomena of PMMA, whereby the replicated profile is little above the insert profile.

The interferometry fringes wavefront was applied in the optical components to analyze the influence of replication errors. The interferogram of the mold and the PMMA sample is in Fig. 15. Figure 15a shows the machined copper mold aspherical wavefront profile, forming perfectly concentric fringes at the mold. Otherwise, Fig. 15b shows an optical aberration of the aspherical wavefront. The wavefront frames at the first Fresnel lens zone (center) were geometrically disformed due to the PMMA warpage surface tension. The other well done performed zones do not find any aberration.

The constant width Fresnel lens construction was quite necessary to understand the geometric influence on the replication process. Figure 16a and b show SEM micrographs of the electrolytic machined mold FrCW250, with very straight and vertical sharp edge zones steps, and no burr appears on the exceptionally smooth mold surface. The respective SEM micrographs of the PMMA sample are in Fig. 16c and d. These images describe the hot-embossing excellent performance of the FrCW250 lens, showing good fidelity of transferring the concentric Fresnel zones lens, with the same straight and vertical step sharp edge of the mold. Hence, these figures indicate that the diamond turning conditions strategy and hot embossing technique used in the experiments were suitable.

Figure 17 shows the 3D general view of 40 concentric Fresnel zones of the electrolytic copper mold and Fig. 17b the respective mold profile with 250 μm constant width. Figure 17c shows 3D of the high-quality replication process of the PMMA sample, and the profile in Fig. 17d, revealing the reverse profile exceptionally similar to the mold, containing 40 zones with 250 μm constant width.

The fidelity height ratio, represented by Eq. (1), and the fidelity width ratio defined by Eq. (2), was plotted in Fig. 18 for the FrCW250. The viscoelastic recovery phenomena only occur under the complete filling of the 3D narrows microstructures replication [13]. In this way, as can be observed, the height of the firsts fifteen zones peaks suffered from the viscoelastic recovery phenomenon and decreasing according

Fig. 15 Interferograms FrCH10. a Electrolytic copper mold. b PMMA replica
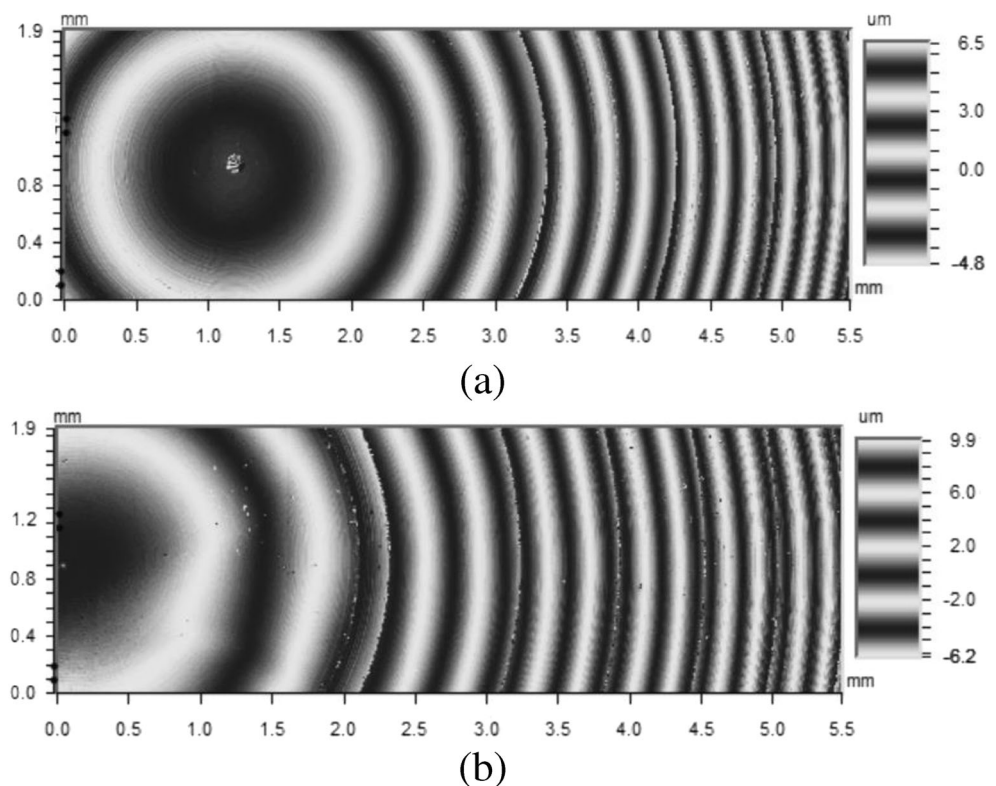
Fig. 16 SEM micrographs characterization of the aspheric FrCW250 profile. **a** General view of constant width Fresnel concentric zones machined on electrolytic copper mold; **b** Detailed view of the mold with sharp steps zone; **c** PMMA hot-embossed general view of the concentric zones Fresnel lens with constant width; **d** PMMA replica showing sharp steps zone
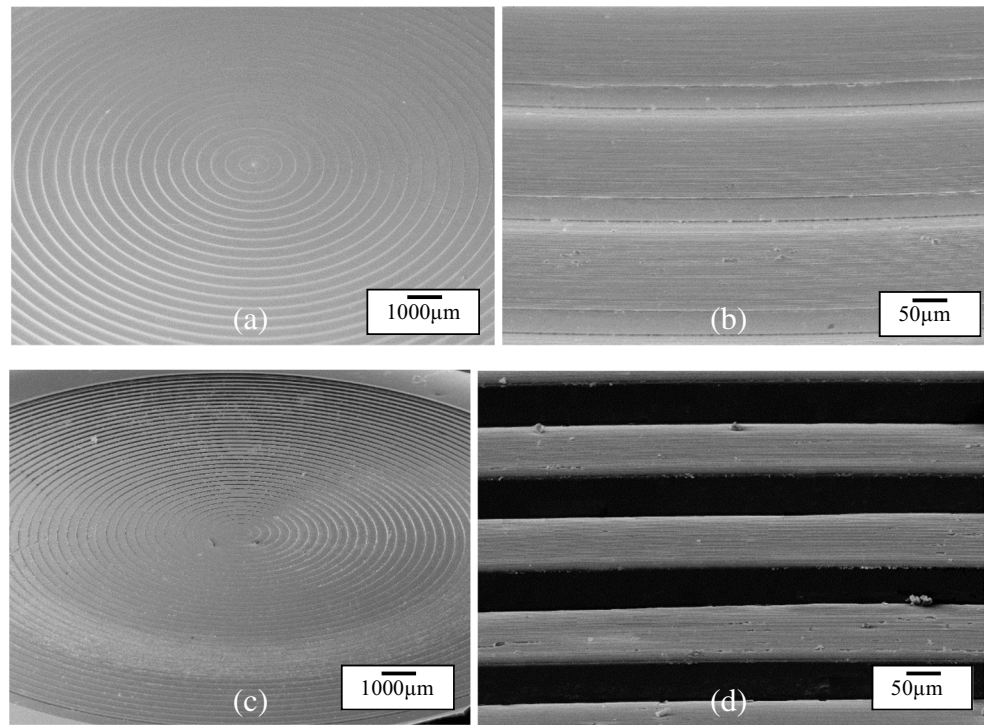
to the outmost zones due to their high aspect ratio that makes filling harder. The width dimensions of zones did not experience the viscoelastic recovery effect.

The structure with a more extensive surface component or significant surface displacement of the initial blank during the process fabrication will produce pronounced recovery or even
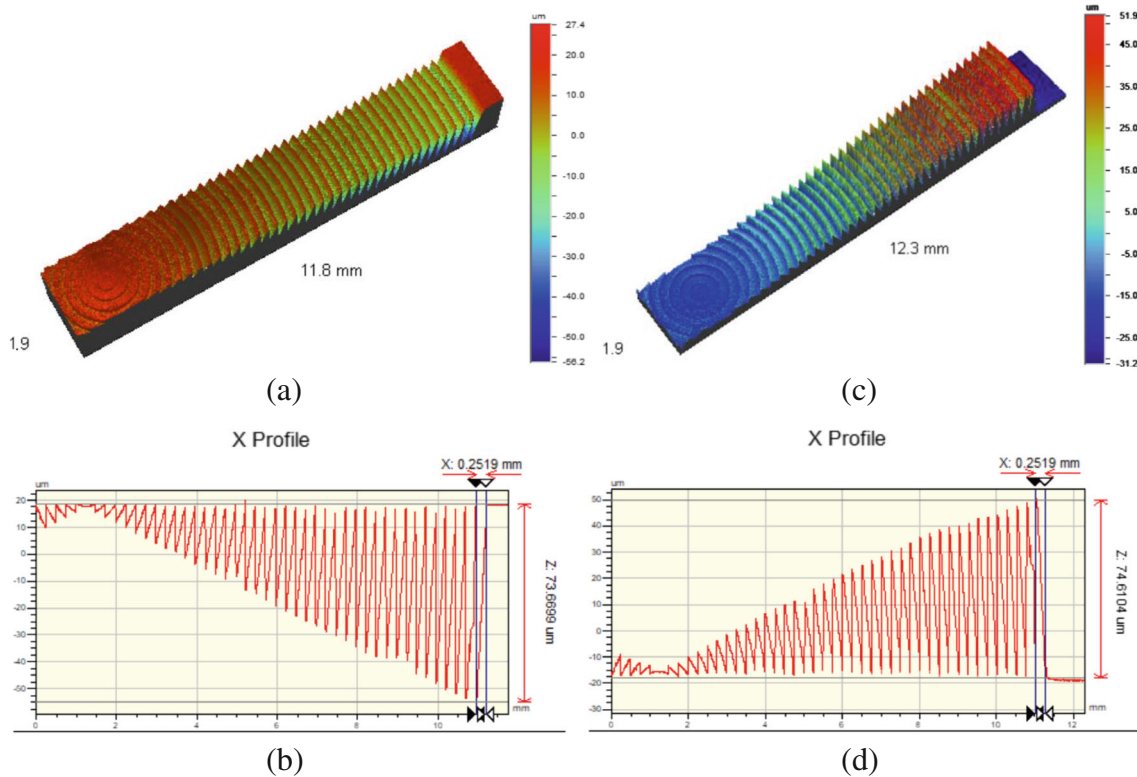
Fig. 17 Characterization of the aspheric FrCW250 lens profile of mold and replica with non-contact optical instrument three-dimensional profilometer. **a** 3D general view of 40 Fresnel zones electrolytic copper mold. **b** Profile of the 250 μm constant width with 40 zones of the mold. **c** 3D general view of 40 Fresnel zones of PMMA replica. **d** Profile 250 μm constant width 40 zones of PMMA replica

Fig. 18 Graphic of width and height fidelity ratio of the 40 zones FrCw250
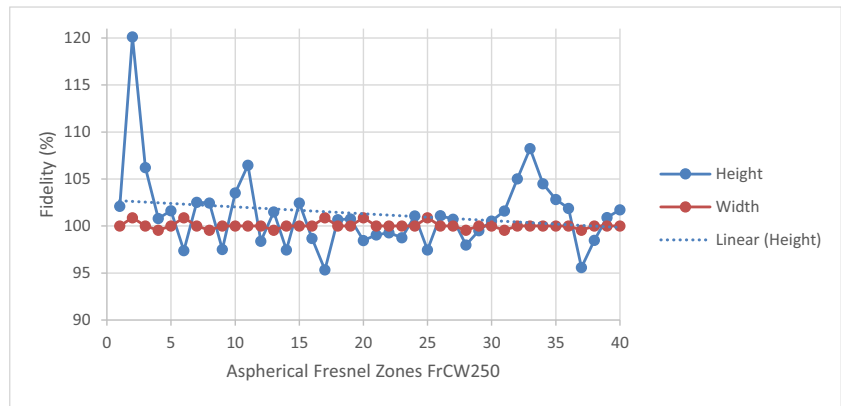
warpage at the workpiece. Geometric forms have a considerable influence on the filling effect of µDOEs affecting the level of accumulated stress in polymer and its corresponding elastic recovery.

Figure 19 shows the overlapped profiles plotted of FrCW250 mold and replica have had the exported 3D non-contact profilometer points. Figure 19a first zones and Fig. 19b second zone magnified, showing the polymer elastic recovery phenomena of PMMA, reaching, in this case, 120%

of the height of the mold. For these zones, it can realize that the PMMA profile is always above of mold profile.

The viscoelastic recovery depends on the form of each 3D microstructure, which will generate standard stress produced by the thermoforming process owing to its exclusive shape. The dependency is related to the part's size, which intrinsically determines the layer's dislocation of the superficial necessary to construct a shape pattern. In this case, the surface area obtained for the FrCW250 lens was $S = 321.035$ mm^2, and

Fig. 19 Profile of FrCW250 mold and replica. a First zones and b second zone magnified showing the polymer elastic recovery phenomena of PMMA
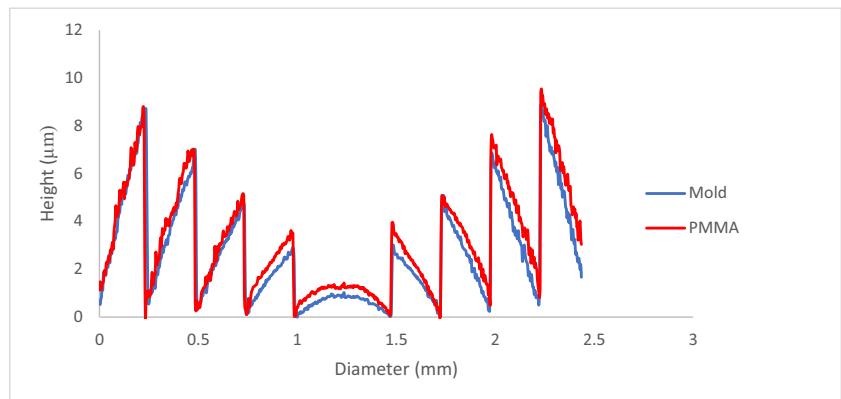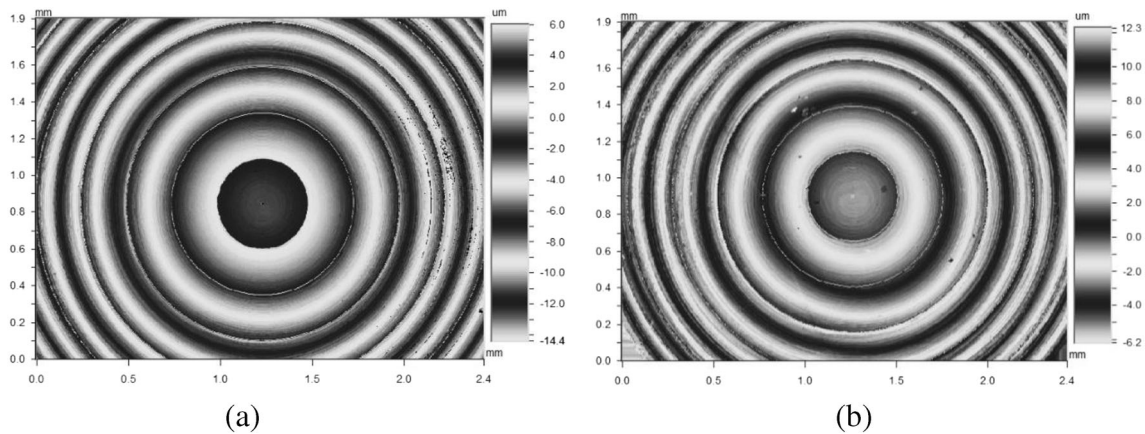

(a)
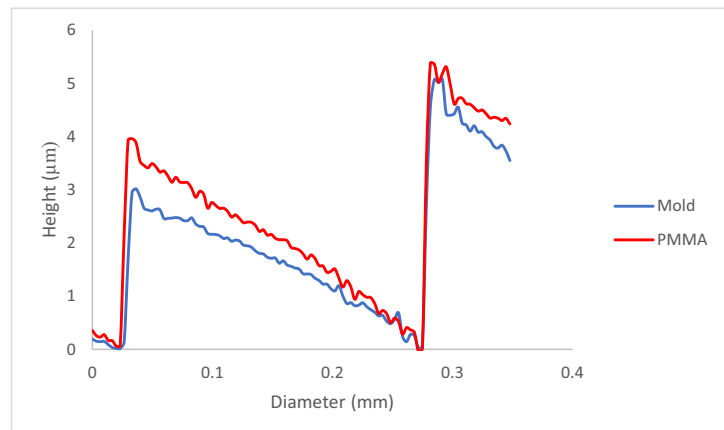
(b)

Fig. 20 Interferograms fo the FrCW250 lens. **a** Electrolytic copper mold. **b** PMMA replica

volume $V = 7.081$ mm^3, so the surface area/volume ratio calculated was 41.15 mm^{-1}. Hence, comparing to FrCH10, fewer stresses were generated on the surface layer, owing to the lower surface area/volume ratio. The surface behavior of the mechanical and optical properties of the lens material, in this case, is the majority defined by the small displacement of the substrate.

Therefore, no optical aberrations appeared in the molded FrCW250, as can be seeing in Fig. 20. At the interferogram analyses of FrCW250 in copper mold Fig. 20a and the respective PMMA replica Fig. 20b, the fringes appear good performed with white and black concentric annular rings, free of optical aberrations.

5 Conclusions

An establishment of the hot embossing manufacturing capability to produce 3D aspheric Fresnel surface microstructures employing a proposed metrology methodology to inspection follows the summarized conclusion below:

1) For all measurements realized at 3D non-contact profilometer indicated that the roughness average (Sa), root-mean-square roughness (Sq), and maximum roughness (St) value of hot-embossed Fresnel microlenses replica was smaller than that of copper mold insert and is comparable with that of excellent optical components in practical use. The proposed method shows a single-point diamond turning deterministic nature to achieve a submicrometer level on the lenses' geometry accuracy and surface roughness in the nanometer level, accomplishing a smooth mirrored surface. Comparing the roughness (Sq) results of the PPMA replica with the device working at a wavelength of 632.8 nm, which corresponds to a ratio reached approximately $\lambda/106$. The benefits of excellent surface integrity directly influence

the filling effect and the lenses' transmittance's excellent performance.

2) Hot-embossing technology allied to the extremely low surface roughness outcomes were essential to replicate high-quality fidelity complex microstructures. Fresnel lenses fabricated with vertical sharp edge walls face different aspect ratios in each zone since it was necessary to use a specific combination of time, temperature, and pressure. The cycle periods of 25 min were essential and suitable combining parameters of the temperature of 120 °C and 150 BAR pressure, to replicate the lens zones, with at least 98% fidelity to Fresnel's FrCH10 and 95% fidelity to FrCW250, both filling occur without demold damage at the crests, and the average height fidelity accuracy was in the submicron level.

3) Thermoplastics polymer, like PMMA, exhibits viscoelastic recovery properties, including stress relaxation at the demold stage and deformation recovery. Viscoelasticity recovery is a phenomenon intrinsically predominant to polymers and complicated to control or cut out its effects. Among several factors that provide the viscoelastic recovery, this work demonstrated that the part's size is responsible directly for the displacement of the superficial layer, influencing the surface/substrate residual stresses producing accentuated recovery of the piece. Therefore, the polymer recovery depends on geometry structure influence since the surface stresses in the corners and edges are locally high. The ratio of surface area/volume is for the FrCH10 = 195.967 mm^{-1} and FrCW250 = 41.15 mm^{-1}, and due to this fact, FrCH10 has more considerable surface tension causing prominent elastic recovery behavior that ranges from a few dozens to hundreds of nanometers. Therefore, filling the lens with constant height FrCH10, recovery behavior was omnipresent, showing elastic condition the PMMA for the most peaks in comparison to constant width FrCW250, and will directly influence the action of the mold filling, as the

surface stresses influenced by geometry and the ratio of surface area/volume.

4) The larger quantity of substrate material in the first zone of FrCH10 produced non-uniform retraction/warpage of the microstructures, causing aberration in the fringe's analysis. Due to the geometric form of FrCW250, the warpage did not occur consequently, making the part free of optical aberration.

The present study provided knowledge for future work by establishing the understanding between the Fresnel microlens manufacturing process correlating to the optical performance effects. Further work will investigate injection molding and paraxial metrology. It will allow us to have more data to compare the same fine microgeometry methods of aspheric Fresnel lens and evaluate the replication fidelity for different fabrication processes.

Author contribution All authors contributed to the study conception and design. Material preparation, literature review, writing, discussion, data collection, and analysis got performed by João Paulo Colafemina and Renato Goulart Jasinevicius. João Paulo Colafemina and Marcel Dib Militão made the development discussion and concept of the LF2020 software, including its discussion and sketches. João Paulo Colafemina wrote the first draft of the manuscript and all authors commented on previous versions of the manuscript. All authors read and approved the final manuscript.

Data availability The datasets generated during and analyzed during the current study are available from the corresponding author on reasonable request.

Declarations

Ethics approval and consent to participate   Not applicable.

Consent for publication   Not applicable.

Conflict of interest   The authors declare no competing interests.

References

1. Joo JY, Lee SK (2009) Miniaturized TIR fresnel lens for miniature optical LED applications. Int J Precis Eng Manuf 10:137–140. https://doi.org/10.1007/s12541-009-0038-8

2. Krizmanic J, Morgan B, Streitmatter R, Gehrels N, Gendreau K, Arzoumanian Z, Ghodssi R, Skinner G (2005) Development of ground-testable phase fresnel lenses in silicon. Exp Astron 20:299–306. https://doi.org/10.1007/s10686-006-9030-9

3. Zhang X, Huang R, Liu K, Kumar AS, Shan X (2018) Rotating-tool diamond turning of Fresnel lenses on a roller mold for manufacturing of functional optical film. Precis Eng 51:445–457. https://doi.org/10.1016/j.precisioneng.2017.09.016

4. Huang R, Zhang X, Kumar AS, Liu K, Rahman M (2017) Profile evaluation of radial Fresnel lens directly machined on roller molds by rotating-tool diamond turning. Precis Eng 50:44–52. https://doi.org/10.1016/j.precisioneng.2017.04.012

5. Peng L, Deng Y, Yi P, Lai X (2014) Micro hot embossing of thermoplastic polymers: a review. J Micromech Microeng 24:013001. https://doi.org/10.1088/0960-1317/24/1/013001

6. Lin TH, Isayev AI, Mehranpour M (2008) Luminance of injection-molded V-groove light guide plates. Polym Eng Sci 48:1615–1623. https://doi.org/10.1002/pen.21138

7. Roeder M, Guenther T, Zimmermann A (2019) Review on fabrication technologies for optical mold inserts. Micromachines 10. https://doi.org/10.3390/mi10040233

8. Wang J, Yi P, Deng Y, Peng L, Lai X, Ni J (2017) Recovery behavior of thermoplastic polymers in micro hot embossing process. J Mater Process Technol 243:205–216. https://doi.org/10.1016/j.jmatprotec.2016.12.024

9. Shan XC, Maeda R, Murakoshi Y (2003) Micro hot embossing for replication of microstructures. Jpn J Appl Phys Part 1 Regul Pap Short Notes Rev Pap 42:3859–3862. https://doi.org/10.1143/jjap.42.3859

10. Smith WJ (2000) Modern optical engineering, 4th edn. Spie. https://doi.org/10.1036/0071476873

11. Spina R, Walach P, Schild J, Hopmann C (2012) Analysis of lens manufacturing with injection molding. Int J Precis Eng Manuf 13:2087–2095. https://doi.org/10.1007/s12541-012-0276-z

12. Liu C, Li JM, Liu JS, Wang LD (2010) Deformation behavior of solid polymer during hot embossing process. Microelectron Eng 87:200–207. https://doi.org/10.1016/j.mee.2009.07.014

13. Gao Y, Jin P, Liu J, Liu T, Prewett PD, Tan J (2012) Control of polymer recovery during replication of micro-optical elements with continuous relief in fused silica. Microelectron Eng 91:106–111. https://doi.org/10.1016/j.mee.2011.10.008

14. Yan J, Maekawa K, Tamaki J, Kuriyagawa T (2005) Micro grooving on single-crystal germanium for infrared Fresnel lenses. J Micromech Microeng 15:1925–1931. https://doi.org/10.1088/0960-1317/15/10/019

15. Brinksmeier E, Karpuschewski B, Yan J, Schönemann L (2020) Manufacturing of multiscale structured surfaces. CIRP Ann 69:717–739. https://doi.org/10.1016/j.cirp.2020.06.001

16. Leung HM, Zhou G, Yu H, Chau FS, Kumar AS (2010) Diamond turning and soft lithography processes for liquid tunable lenses. J Micromech Microeng 20:025021. https://doi.org/10.1088/0960-1317/20/2/025021

17. Bäumer S (2010) Handbook of plastic optics, 2nd edn. Wiley-VCH Verlag GmbH & Co. KGaA, Weinheim. https://doi.org/10.1002/9783527635443

18. Zhang HL, Ong NS, Lam YC (2007) Effects of surface roughness on microinjection molding. Polym Eng Sci 47:2012–2019. https://doi.org/10.1002/pen.20904

19. Der Chien R (2006) Hot embossing of microfluidic platform. Int Commun Heat Mass Transfer 33:645–653. https://doi.org/10.1016/j.icheatmasstransfer.2006.01.017

20. Deshmukh SS, Goswami A (2019) Hot embossing of polymers—a review. Mater Today Proc 26:405–414. https://doi.org/10.1016/j.matpr.2019.12.067

21. Sha B, Dimov S, Griffiths C, Packianather MS (2007) Micro-injection moulding: factors affecting the achievable aspect ratios. Int J Adv Manuf Technol 33:147–156. https://doi.org/10.1007/s00170-006-0579-2

22. Sha B, Dimov S, Pham D (2005) Study of factors affecting aspect ratios achievable in micro-injection moulding. Proc First:1–4

23. Griffiths CA, Dimov SS, Brousseau EB, Hoyle RT (2007) The effects of tool surface quality in micro-injection moulding. J Mater Process Technol 189:418–427. https://doi.org/10.1016/j.jmatprotec.2007.02.022

24. Eladl A, Mostafa R, Islam A, Loaldi D, Soltan H, Hansen HN, Tosello G (2018) Effect of process parameters on flow length and flash formation in injection moulding of high aspect ratio polymeric micro features. Micromachines 9. https://doi.org/10.3390/mi9020058

25. Becker H, Heim U (2000) Hot embossing as a method for the fabrication of polymer high aspect ratio structures. Sensors Actuators A Phys 83:130–135. https://doi.org/10.1016/S0924-4247(00)00296-X

26. Lin L, Cheng YT, Chiu CJ (1998) Comparative study of hot embossed micro structures fabricated by laboratory and commercial environments. Microsyst Technol 4:113–116. https://doi.org/10.1007/s005420050109

27. Cirino GA, Granado RM, Mohammed-Brahim T, Jasinevicius RG (2017) Assessment of replication fidelity of optical microstructures by hot embossing. Int J Adv Manuf Technol 88:303–316. https://doi.org/10.1007/s00170-016-8757-3

28. Crawford RJ (1998) Plastics engineering. Elsevier, Amsterdam. https://doi.org/10.1016/B978-0-7506-3764-0.X5000-6

29. Groover MP (2019) Fundamentals of modern manufacturing: materials, processes, and systems 7th Edition, Wiley. WileyCom n.d. https://www.wiley.com/en-us/Fundamentals+of+Modern+Manufacturing%3A+Materials%2C+Processes%2C+and+Systems%2C+7th+Edition-p-9781119475217

30. Lee CS, Kang CG, Youn SW (2010) Effect of forming conditions on linear patterning of polymer materials by hot embossing process. Int J Precis Eng Manuf 11:119–127. https://doi.org/10.1007/s12541-010-0015-2

31. Shan X, Liu YC, Lam YC (2008) Studies of polymer deformation and recovery in micro hot embossing. Microsyst Technol 14:1055–1060. https://doi.org/10.1007/s00542-007-0486-y

32. Dib MHM, Colafemina JP (2019) Lentes de Fresnel Anesféricas Versão 2020 - Certificado de Registro de Programa de Computador. 2529. BR512019001216–0

33. Gao W, Haitjema H, Fang FZ, Leach RK, Cheung CF, Savio E, Linares JM (2019) On-machine and in-process surface metrology for precision manufacturing. CIRP Ann 68:843–866. https://doi.org/10.1016/j.cirp.2019.05.005

34. Guan B, Cherrill M, Pai JH, Priest C (2019) Effect of mould roughness on injection moulded poly (methyl methacrylate) surfaces: roughness and wettability. J Manuf Process 48:313–319. https://doi.org/10.1016/j.jmapro.2019.10.024

35. Ligia G, Deodato R (2009) Physicochemical behavior and supramolecular organization of polymers. Springer Netherlands. https://doi.org/10.1007/978-1-4020-9372-2